RSC Advances

PAPER

View Article Online
View Journal | View Issue

Cite this: *RSC Adv.*, 2022, **12**, 21681

MIL-53 and its OH-bonded variants for bio-polyol adsorption from aqueous solution

Na Cao,[ab] Jiayi Liu,[ac] Yuecheng Wang,[ab] Yingwu Zhou,[ab] Meng Zhao,[ab] Yujie Ban *[ab] and Weishen Yang [ab]

The adsorption of bio-polyols from dilute aqueous solution is important but faces challenges in the sustainable bio-refinery process. One solution to increase adsorption efficiency is to leverage host–guest interactions between the polyols and materials to grant a preference for polyols. In this study, we synthesized MIL-53 and diverse OH-bonded variants, and studied their adsorption properties towards ethanediol, 1,3-propanediol and glycerol in water. Among the four materials, OH–MIL-53 exhibited fast adsorption kinetics and high capacity, and could be completely regenerated through ethanol elution. Hydrophobic interactions between the alkyl chains of the polyols and the organic linkers of OH–MIL-53 and hydrogen bonding interactions between their OH groups were identified. The synergistic effect of the host–guest interactions is responsible for the unique adsorption performances of OH–MIL-53 towards polyols, and particularly for 1,3-propanediol.

Received 21st May 2022
Accepted 14th July 2022

DOI: 10.1039/d2ra03203a

rsc.li/rsc-advances

1 Introduction

The growing concern about the negative impact of CO_2 emissions has triggered a transition of the industrial paradigm from mostly petro-based sources to alternative bio-based sources. Short-chain polyols such as ethanediol and propanediols are important bio-based chemical platforms, with their market volume reaching a million tons per year.[1,2] Take 1,3-propanediol as an example. As a subclass of "smart drop-in" bio-chemicals, 1,3-propanediol is mainly used as a solvent, coolant, antifreeze agent, humectant for skincare products, and more importantly, a monomer for polyesters, polyethers, and polyurethanes. The current biochemical conversion routes frequently yield polyols in aqueous solution, with the concentration of the products generally lower than 70 g L^{-1},[3] and their separation is a major bottleneck.

Compared with traditional distillation that needs a large energy input for the evaporation of a large amount of water, the dehydration pervaporation technique using membranes is energy-efficient and can realize water removal from polyols.[4–9] It is therefore a good "polishing" method for chemicals and especially for chemicals with water contents lower than 10 wt%. For example, we recently reported hetero-lattice intergrown MOF membranes that showed a water/ethanediol separation factor as high as 13 000 towards a 90/10 ethanediol/water solution.[9] Membrane pervaporation can realize the deep dewatering of high-concentration organic chemicals but is not suitable for removing a great deal of water from low-concentration polyols because of the huge membrane cost. For low-concentration aqueous polyol systems, one complementary solution with economic efficiency is the deployment of suited materials to capture polyols by means of the preference of the materials for polyols. Considering the low volatility of polyols, adsorption based on porous materials under liquid-phase conditions enjoys priority for the recovery of polyols from water but faces challenges because of the strong hydrogen bonds identified in the polyol–water system.[3,10] One solution to the polyol extraction from water is to take advantage of the weak hydrophobicity derived from short alkyl chains.[11] Another way forward might be to focus on some functional groups appended into (porous) materials that can provide delicate host–guest interactions.[12] For example, the reversible binding of boronate with diol motifs has stimulated the development of boronic acid-functionalized stationary phases in chromatographic techniques that were utilized for selective saccharide separation.[13–15] Additionally, intramolecular hydrogen bonding such as O–H···O–H that is common in selective adsorption provides inspiration for the recovery of polyols from water.[16,17] However, adsorbents with high capacity along with recyclability towards high-boiling-point polyols have been rarely reported.[11,18–22]

Connecting metal ions and organic linkers in a periodic network affords metal–organic frameworks (MOFs) with permanent high porosity. Their modular chemistry encourages the diversity of MOFs.[23–26] The point is that we can regulate the linker part for desirable functionality.[27–29] Particularly, the unique adsorption properties of MOFs often stem from the

[a]State Key Laboratory of Catalysis, Dalian Institute of Chemical Physics, Chinese Academy of Sciences, Dalian, 116023, China. E-mail: yjban@dicp.ac.cn
[b]University of Chinese Academy of Sciences, Beijing, 100049, China
[c]Zhang Dayu School of Chemistry, Dalian University of Technology, Dalian, 116024, China

linkers' propensity for host–guest interactions, hydrogen bonding,[30] CH–π,[31] π–π[32] and acid–base interactions.[33] To create a solution for polyol adsorption, MOFs with diverse linkers might be a candidate due to their kinetics, equilibrium capacity and recyclability.

MIL-53 (Al), with the combination of Al^{3+} and terephthalate linkers resulting in one-dimensional channels, has gained great prominence in adsorption and separation, and ranks among the A-list MOFs due to its ultrastability.[34] Terephthalates are important platform chemicals for yielding functional variants. In this work, we synthesized various OH-bonded MOF variants *via* the reaction of Al^{3+} and functional linkers, and investigated the adsorption properties of MIL-53 and OH-bonded variants for polyols in aqueous solutions at a wide concentration range (10–500 g L^{-1}). OH–MIL-53 shows fast adsorption kinetics and high capacity at room conditions. We attributed this excellent adsorption behavior to the host–guest interactions between the polyols and materials. Furthermore, we found that OH–MIL-53 could be completely regenerated, with adsorption capacity analogous with that of the fresh adsorbent.

2 Experimental

2.1 Chemicals

All chemicals were commercially supplied and directly used in the experiments. Terephthalic acid (TA, $C_8H_6O_4$, 98%), 2,5-dihydroxyterephthalic acid (DHTA, $C_8H_6O_6$, 98%) and aluminum nitrate nonahydrate ($Al(NO_3)_3\cdot 9H_2O$, ≥98%) were purchased from Sigma-Aldrich Inc. 2-(Dihydroxyboryl) terephthalic acid (DHBTA, $C_8H_7BO_6$, 98%) was purchased from Shanghai Macklin Biochemical Co., Ltd. Aluminum chloride hexahydrate ($AlCl_3\cdot 6H_2O$, ≥97%), *N*,*N*-dimethylformamide (DMF, C_3H_7NO, ≥99.5%), acetone ($(CH_3)_2CO$, ≥99.5%) and absolute ethanol (C_2H_6O, ≥99.7%) were purchased from Sinopharm Chemical Reagent Co., Ltd. Ultrapure water was supplied by Hangzhou Wahaha Group Co., Ltd. 2-Hydroxyterephthalic acid (HTA, $C_8H_6O_5$, ≥98%), ethanediol ($C_2H_6O_2$, ≥99%), 1,3-propanediol ($C_3H_8O_2$, 98%), and glycerol ($C_3H_8O_3$, ≥99%) were supplied by Shanghai Aladdin Biochemical Technology Co., Ltd. Stainless steel net (SSN) substrates (3AL3, thickness: 0.37 mm) were purchased from Bekaert (China) Co. These consisted of top, intermediate and bottom layers with average pore sizes of 6.5 μm, 2.0 μm and 6.5 μm, respectively. SSN substrates were cut into discs with a diameter of 19 mm for use.

2.2 Synthesis of MIL-53 and its OH-bonded variants

MIL-53, OH–MIL-53 and $B(OH)_2$–MIL-53 were constructed according to previous literature.[35,36] Briefly, 10.2 mmol TA (or HTA or DHBTA) was dissolved in 30 mL DMF, and was slowly added dropwise to an aqueous solution of $Al(NO_3)_3\cdot 9H_2O$ (with 21 mmol of the salt dissolved in 30 mL water) at room temperature. The metal–linker reaction was activated under reflux of the solution at 90 °C. Over a span of 36 h, the precipitate was recovered *via* centrifugation and dried at 80 °C in air. Then, the solids were washed with absolute ethanol in a Soxhlet extractor at 100 °C for 48 h for solvent exchange. Finally, the solids were dried at 120 °C for 24 h with continuous evacuation in an oven.

$(OH)_2$–MIL-53 was synthesized by a solvothermal method.[37] The mixture, obtained by dissolving $AlCl_3\cdot 6H_2O$ (6.2 mmol) and DHTA (6.2 mmol) in a 60 mL DMF–water mixed solvent (3 : 1, v/v), was transferred to a teflon-lined steel autoclave and heated at 150 °C for 24 h. After briefly washing with DMF at ambient conditions, the product was re-soaked in 60 mL DMF, transferred to a teflon-lined steel autoclave and heated at 150 °C for 5.5 h. The product was recovered by centrifugation, briefly washed with acetone and dried at 120 °C overnight. Ultimately, the as-synthesized product was activated by calcination in air, following protocols analogous with our previous study.[38]

Notably, in our lab, we have a special ledger to record the use of hazardous chemicals. Toxic chemical waste was segregated by compatibility, stored in special containers, and transferred to a qualified professional company for harmless disposal.

2.3 Characterization

The powder X-ray diffraction (XRD) patterns of MIL-53 and its OH-bonded variants were collected on a Rigaku instrument (D/MAX 2500/PC) with a scan speed of 5° min^{-1} and a 2θ range of 2–50°. The setup of the instrument was as follows: the acceleration voltage at 40 kV and current at 200 mA. Here, the wavenumber of Cu Kα radiation is 0.154 nm. The morphology and particle size of the sample were probed using scanning helium ion microscopy (SHIM, ORION NanoFab). Thermogravimetric (TG) analysis was performed on a Netzsch STA449F3 instrument with a ramp rate of 5 °C min^{-1} from 40 °C to 1000 °C in air (flow rate: 100 mL min^{-1}). N_2 adsorption measurements were carried out on a Micromeritics ASAP 2020Plus instrument at 77 K. According to the N_2 adsorption isotherms measured, the Brunauer–Emmett–Teller (BET) surface area and pore size distribution were obtained. The Fourier-transform infrared spectroscopy (FTIR) spectra of the samples in the mode of attenuated total reflection were recorded on a Nicolet 6700 spectrometer, with 32 scans at a resolution of 4 cm^{-1}. A BRUKER VERTEX 80v vacuum FTIR spectrometer was used to obtain the *in situ* spectra of the samples from 50 °C to 150 °C by temperature programming. Contact angle (CA) measurements were carried out on a Kruss DSA 100 analyzer. Given that MIL-53 and its variants can hardly be pressed into a pellet without an adhesive under moderate pressure (∼6 bar), we carefully scrubbed the powder on an SSN substrate by hand for the CA measurements.

2.4 Adsorption of polyols from the aqueous solution

Prior to polyol adsorption, MIL-53 and its OH-bonded variants were evacuated at 120 °C overnight to get rid of water molecules adsorbed in the pores.

The adsorption of polyols on diverse dehydrated MIL-53 materials was performed at room temperature. For example, 30 mg OH–MIL-53 was added to a 500 μL aqueous ethanediol solution, followed by continuous blending using an automatic

mixer control system (IKA VORTEX GENIUS 3). After 20 min, the solid–liquid mixture was split by centrifugation. Then, the concentration of ethanediol in the supernatant was detected by liquid chromatography (LC, Agilent 1260) with an RI detector. The chromatographic column was SUGAR SC1011 from Shodex. The uptake amount of ethanediol was calculated using the formula $q_t = (VC_0 - VC_t)/m$, where q_t is the adsorption capacity (mg g^{-1}), V is the volume of the adsorbate solution (L), C_0 and C_t are the initial concentration and terminated concentration of the polyol solution (g L^{-1}), respectively, and m is the mass of the adsorbent (g).

2.5 Regeneration of OH–MIL-53

After polyol adsorption, OH–MIL-53 was washed with ethanol at 100 °C for 24 h in a Soxhlet extractor, and dried at 120 °C for 24 h in a vacuum oven for regeneration. Then, the regenerated OH–MIL-53 was applied in cyclic polyol adsorption.

3 Results and discussion

3.1 Characterization of MIL-53 and its OH-bonded variants

The powder XRD patterns show featured diffraction peaks of the OH-bonded variants in agreement with the simulated pattern of MIL-53. The iso-reticular crystalline structure of the variants was accordingly validated, showing the great tolerance of the MIL-53 lattice for the bulky substituent group of the linker (Fig. 1a). MIL-53 and its OH-bonded variants can spontaneously adsorb moisture in air. The bending vibration mode of water molecules is clearly identified at 1680–1630 cm^{-1} in the FTIR spectra (Fig. 1b). Considering the weight loss below 100 °C as a result of water desorption, as shown in the TG curves of MIL-53 and its variants (Fig. 3), the uptake amount of water in the adsorbents was quantified as follows: MIL-53·0.4H_2O, OH–MIL-53·0.5H_2O, $(OH)_2$–MIL-53·0.5H_2O and $B(OH)_2$–MIL-53·0.5H_2O. From the FTIR spectra in Fig. 1b, we can also discern a broad band ranging from 3700 to 3000 cm^{-1}, which is attributed to the stretching vibration mode of hydrogen bonds between adsorbed water molecules as well as the water and decorated OH groups. MIL-53 and its variants exhibit type-I isotherms for N_2 adsorption at 77 K, without hysteresis between the adsorption and desorption branches, which validates their permanent microporosity (Fig. 1c). The Brunauer–Emmett–Teller (BET) surface areas amount to 1441, 1431 and 629 m^2 g^{-1} for MIL-53, OH–MIL-53 and $B(OH)_2$–MIL-53, respectively (Table 1), showing a reduction with the size of the substituent group in the linker. The BET surface area of $(OH)_2$–MIL-53 is 238 m^2 g^{-1}, indicating

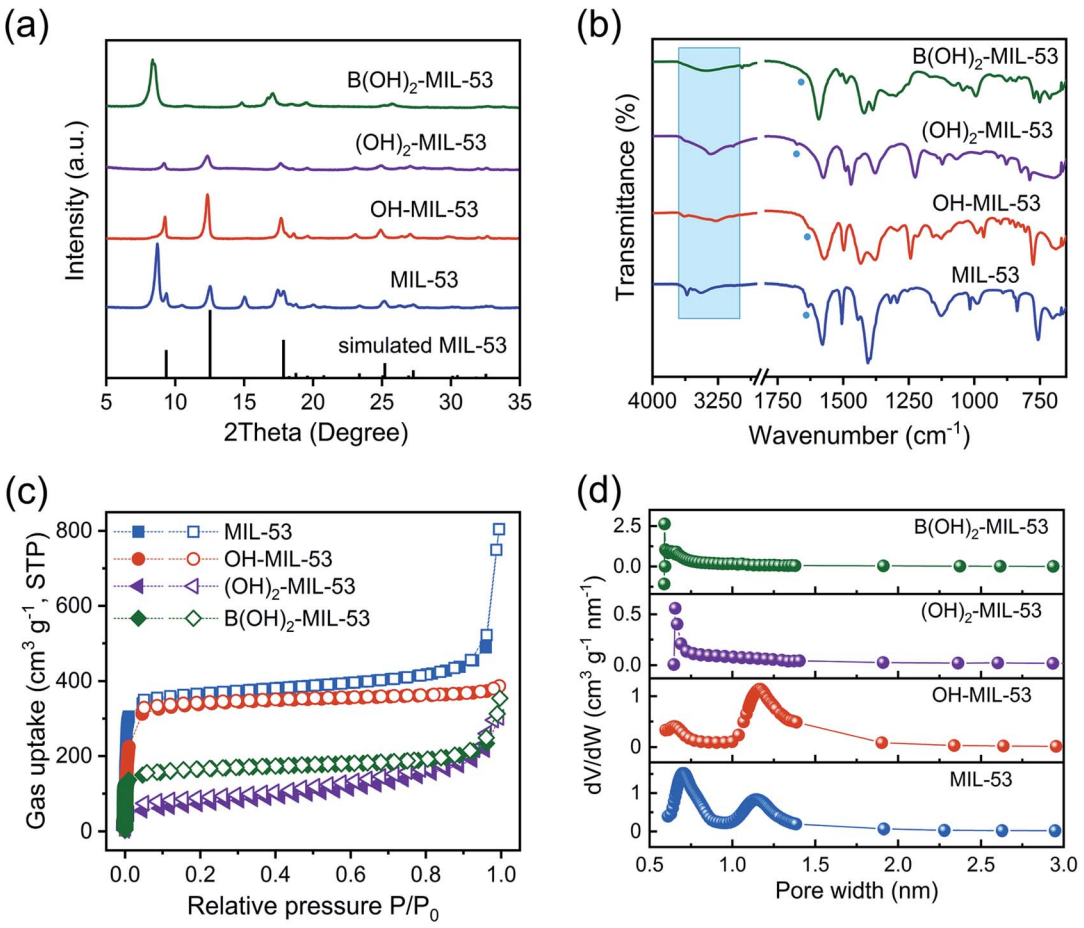

Fig. 1 XRD patterns (a) and FTIR spectra (b) of MIL-53 and its OH-bonded variants. (c) N_2 adsorption (solid symbol) and desorption (open symbol) isotherms at 77 K. (d) Pore size distribution calculated by the Horvath–Kawazoe method.

the blocking effect of "*para*-OH" on the interior space accessible to N_2 molecules. Moreover, the pore size distributions of MIL-53 and its variants were determined by the Horvath–Kawazoe method (Fig. 1d). A hierarchy in the micropores emerges in MIL-53 and OH–MIL-53, with one population locating at around 0.65 nm and the other locating at around 1.15 nm. With the *para*-OH and $B(OH)_2$ groups bonded into the skeleton, the micropore of the variants at *ca.* 1.15 nm diminishes, alongside a sharp micropore at *ca.* 0.65 nm. We also find that the maximum pore volume of MIL-53 and its variants shows the order of MIL-53 > OH–MIL-53 > $B(OH)_2$–MIL-53 > $(OH)_2$–MIL-53, which is consistent with the sequence of the BET surface area. SHIM images (Fig. 2a–d) indicate that MIL-53 and its variants show an irregular corn-like morphology. The particle size distributions were fitted by the Gaussian curve (Fig. 2e–h). The maximum dimensions of the particles are around 250 nm, 500 nm, 100 nm and 750 nm for MIL-53, OH–MIL-53, $(OH)_2$–MIL-53 and $B(OH)_2$–MIL-53, respectively. According to our previous study,[38] the dimension of the particles falling in the nanometer level cannot affect the adsorption kinetics of polyols, which is also proved in the following study.

3.2 Polyol adsorption properties on MIL-53 and its OH-bonded variants

MIL-53 and its variants were implemented in the testing of polyol adsorption from water at room temperature. This study

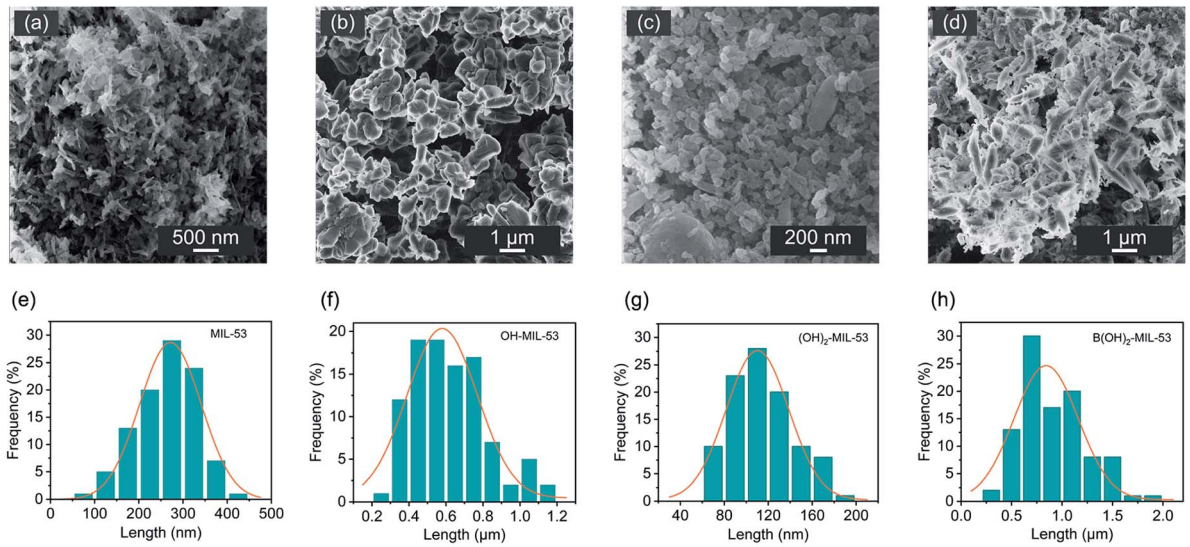

Fig. 2 SHIM images of MIL-53 (a), OH–MIL-53 (b), $(OH)_2$–MIL-53 (c) and $B(OH)_2$–MIL-53 (d). Particle size distribution analyzed by the ImageJ software (e–h).

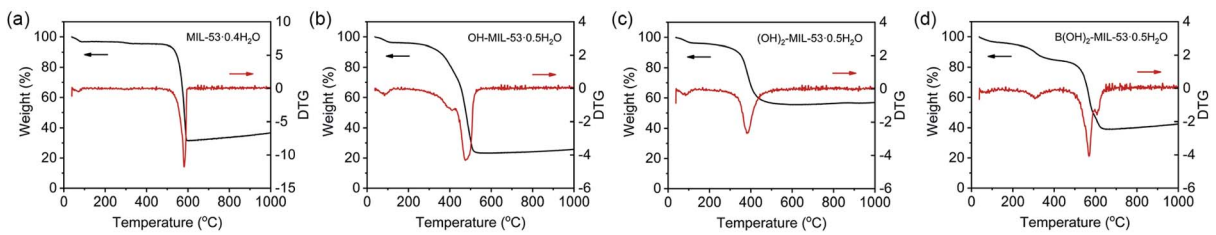

Fig. 3 TG curves of MIL-53 and its variants.

Table 1 BET surface area, maximum pore volume and pore width of MIL-53 and its variants

Materials	BET surface area ($m^2\ g^{-1}$)	Maximum pore volume[a] ($cm^3\ g^{-1}$)	Pore width[a] (nm)
MIL-53	1441	0.6406	0.70, 1.14
OH–MIL-53	1431	0.5606	0.65, 1.17
$(OH)_2$–MIL-53	238	0.1613	0.65
$B(OH)_2$–MIL-53	629	0.2967	0.59

[a] Calculated by the Horvath–Kawazoe method.

explores the adsorption properties of polyols in a wide concentration range (10–500 g L^{-1}) for meeting the attributes of various application scenarios in industry. Before the adsorption measurements, MIL-53 and its OH-bonded variants were treated in a hot-vacuum condition to render complete desorption of the water molecules. We firstly studied the adsorption kinetics. Remarkably, the adsorption of 1,3-propanediol takes 10 minutes (excluding the centrifugation time) to reach equilibrium on MIL-53 and OH–MIL-53 at the concentrations of 50 g L^{-1} and 200 g L^{-1} (Fig. 4). Generally, polyol adsorption on resins, MOFs and ZSM-5 ref. 11,21,39,40 needs 4–24 h to reach adsorptive equilibrium based on earlier literature. Clearly, MIL-53 and OH–MIL-53 enjoy advantages in terms of adsorption kinetics, as they are not sensitive to particle size.

Polyol adsorption at moderately high concentrations (300, 400 and 500 g L^{-1}) was typically conducted on MIL-53 and its OH-bonded variants. As shown in Fig. 5a, MIL-53 and OH–MIL-53 display noticeable ethanediol uptake, whereas $(OH)_2$–MIL-53 and $B(OH)_2$–MIL-53 can hardly adsorb ethanediol from the aqueous solution. In the case of an ethanediol concentration of 500 g L^{-1}, the saturation uptake of ethanediol on MIL-53 and OH–MIL-53 reaches 269 and 218 mg g^{-1}, respectively, which is much higher than that on $(OH)_2$–MIL-53 (50.5 mg g^{-1}) and $B(OH)_2$–MIL-53 (16.0 mg g^{-1}). MIL-53, relative to OH–MIL-53, can adsorb more ethanediol at the same condition. We speculate that the interior surface area of the materials might be a positive factor. The adsorption properties of 1,3-propanediol on the materials are shown in Fig. 5b. Except for $(OH)_2$–MIL-53, MIL-53 and its OH-bonded variants manifest significant uptake amount for 1,3-propanediol. In the case of a 1,3-propanediol concentration of 500 g L^{-1}, the saturation uptakes of 1,3-propanediol on MIL-53 and OH–MIL-53 are 273 and 278 mg g^{-1}, respectively. OH–MIL-53 exhibits a larger uptake amount for 1,3-propanediol, although the surface area of OH–MIL-53 is slightly lower than that of MIL-53. We speculate that the host–guest interaction between the polyol and OH-bonded materials might be behind this result. Comparatively, MIL-53 and its OH-bonded variants show weak adsorption for glycerol (Fig. 5c). A positive result points to OH–MIL-53, on which the saturation uptake at a glycerol concentration of 500 g L^{-1} was 124 mg g^{-1}.

Surface wettability is an important factor influencing the adsorption properties. We measured the contact angle of polyols on the materials, as shown in Fig. 6. Clearly, glycerol has poor wettability on the surface of the materials, and the CA for glycerol on MIL-53 and its OH-bonded variants was above 110°, which is indicative of the sorption deficiency of glycerol on materials. Inversely, ethanediol and 1,3-propanediol have better wettability on the surface of the materials, which supports the corresponding theoretical adsorption.

We compared the polyol adsorption on MIL-53 and OH–MIL-53 at a concentration of 500 g L^{-1}, as shown in Fig. 7. The adsorption of polyols on both materials follows the order of 1,3-propanediol > ethanediol > glycerol. The 3D molecular structure of the polyols was modelled, as shown in Fig. 8. The largest dimensions of ethanediol, 1,3-propanediol and glycerol molecules, determined to be 3.7, 4.7, and 5.1 Å, respectively, were distinctly shorter than the pore widths of MIL-53 and its variants (more than 5.9 Å). Consequently, the possibility of mismatch between the dimension of the polyols and the pore size of the materials can be ruled out.

Furthermore, the *n*-octanol water partition coefficient (K_{ow}) of the three polyols follows the order of glycerol < ethanediol < 1,3-propanediol, as shown in Table 2. This means that 1,3-propanediol has a weaker hydrophobicity than ethanediol and glycerol, and is prone to escape from water despite the fact that hydrogen bonds form between the polyol and water.[11] Accordingly, if it meets MIL-53 or OH–MIL-53, the hydrophobic interaction between the short alkyl chains and organic linkers of the MOFs drives the superior adsorption of 1,3-propanediol on MIL-53 and especially on OH–MIL-53.

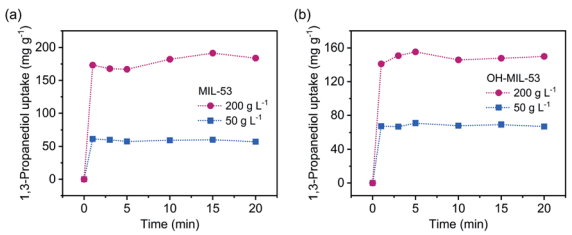

Fig. 4 Kinetic adsorption curves of MIL-53 (a) and OH–MIL-53 (b) at the concentrations of 50 g L^{-1} and 200 g L^{-1}.

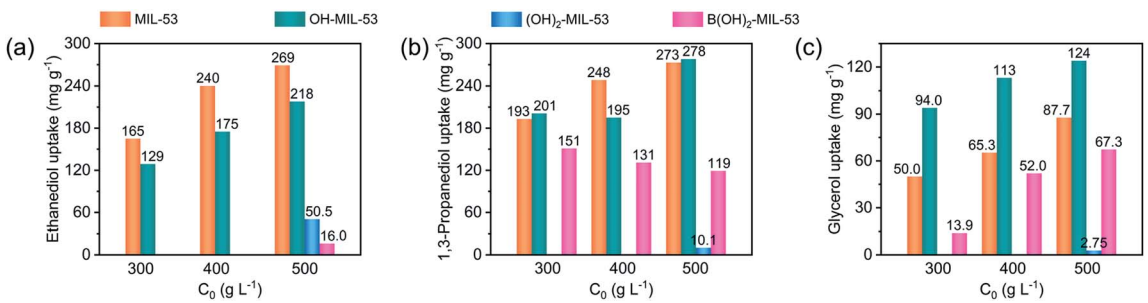

Fig. 5 Single-component adsorption of ethanediol (a), 1,3-propanediol (b), and glycerol (c) on MIL-53 and its variants from high-concentration aqueous solution. The absence of columns means no adsorption experiments conducted at lower concentration owing to poor performances of the materials at 500 g L^{-1}.

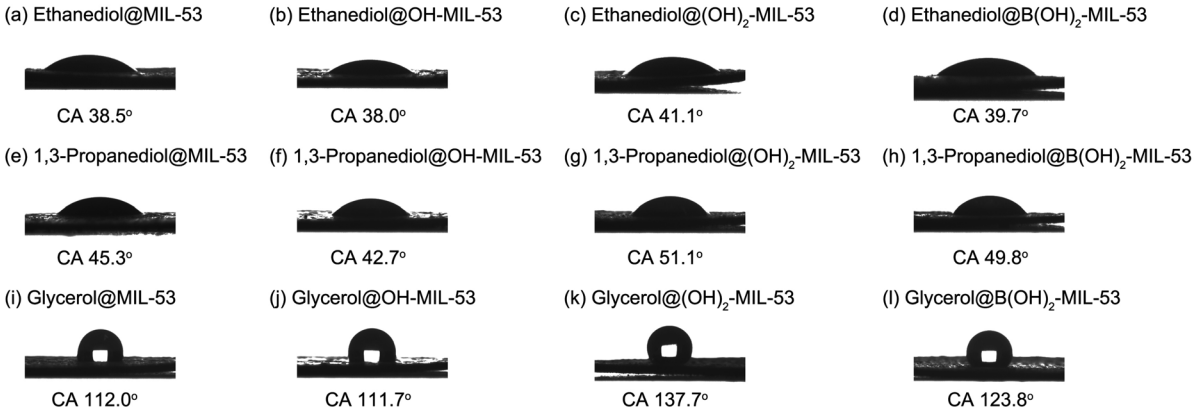

Fig. 6 Contact angle images for polyol droplets on MIL-53 and its OH-bonded variants.

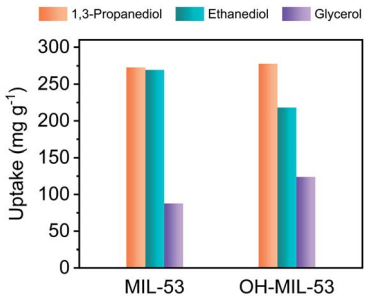

Fig. 7 Polyol adsorption on MIL-53 and OH–MIL-53 (concentration: 500 g L^{-1}).

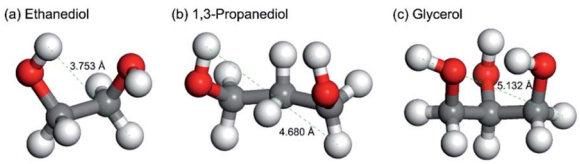

Fig. 8 The 3D molecular structures of ethanediol (a), 1,3-propanediol (b) and glycerol (c). The largest dimension determined by the terminal atoms is marked in the picture.

Table 2 The *n*-octanol water partition coefficient of ethanediol, 1,3-propanediol and glycerol

Polyols	K_{ow}
Ethanediol	0.0436
1,3-Propanediol	0.0912
Glycerol	0.0174

Polyol adsorption on MIL-53 and OH-bonded MIL-53 was further investigated at extremely low concentrations of polyol solution (10–200 g L^{-1}), which meets the attributes of the biorefinery broth. As shown in Fig. 9, we notice a steep adsorption behavior of polyols on OH–MIL-53. For example, when the initial concentration of the ethanediol solution increases from 50 to 100 and then to 200 g L^{-1}, the ethanediol uptake on OH–MIL-53 ramps up from 36.6 to 72.0 and then to 114 mg g^{-1}, in comparison with the uptake on MIL-53 varying from 29.8 to 43.3 and then to 99.5 mg g^{-1}, respectively. Obviously, OH–MIL-53 is fit to extract ethanediol from very diluted solutions, although its uptake at higher concentrations of ethanediol solution, for instance, 500 g L^{-1}, is suboptimal compared to that of MIL-53. The uptakes of ethanediol and 1,3-propanediol on OH–MIL-53 are 114 and 146 mg g^{-1}, respectively, at a concentration of 200 g L^{-1}, which is superior to that of $B(OH)_2$–MIL-53 (94.8 mg g^{-1} for 1,3-propanediol) under analogous conditions. The uptake amount of polyols on OH–MIL-53 at low concentrations of polyol solution likewise follows the order of 1,3-propandiol > ethanediol > glycerol, as shown in Fig. 10. Nevertheless, the uptake of glycerol on OH–MIL-53 reaches 85.1 mg g^{-1} at a concentration of 200 g L^{-1}, which is far beyond that on MIL-53 (41.9 mg g^{-1}). Notably, from previous literature,[11] the uptakes of 1,3-propanediol on ZSM-5, SIM-1 and ZIF-8 are 93 mg g^{-1} (at a concentration of 242 g L^{-1}), 130 mg g^{-1} (at a concentration of 200 g L^{-1}) and 148 mg g^{-1} (at a concentration of 250 g L^{-1}). Overall, in terms of polyol adsorption, OH–MIL-53 has advantages over zeolites and some well-known MOFs. We speculate that the delicate host–guest interaction between the polyol and OH–MIL-53 might be responsible for this result, which will be discussed in the following section.

3.3 Host–guest interaction between polyol and OH–MIL-53

The *in situ* FTIR spectra of MIL-53 show the real-time desorption of guest molecules (water) in the temperature program, which is consistent with the TG analysis (Fig. 11). The characteristic peak of hydrogen bonding derived from water molecules is weakened gradually with temperature and is absent at 100 °C, which indicates that water was entirely removed when the temperature was raised to 120 °C. The ex-situ FTIR spectra of the MOF materials with the uptake of polyols were utilized to study the host–guest interaction. Since polyol adsorption on MIL-53 and its OH-bonded variants was performed in an aqueous solution, MIL-53 and its OH-bonded variants with polyol uptake were completely dehydrated *via* thermal treatment (120 °C) under vacuum conditions to get rid of the water effect on the FTIR spectra. Fig. 12a shows the significant peak of MIL-53 with the

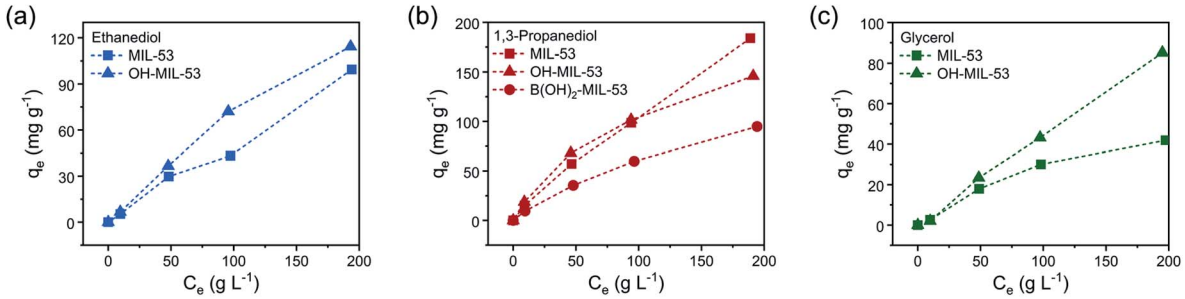

Fig. 9 Adsorption isotherms of ethanediol (a), 1,3-propanediol (b) and glycerol (c) on MIL-53 and its variants at ambient conditions.

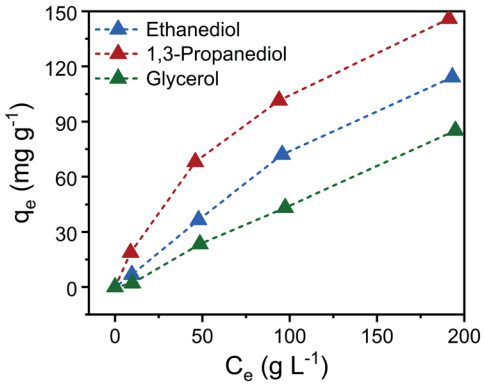

Fig. 10 Adsorption isotherms of polyols on OH–MIL-53 from low-concentration aqueous solution at room temperature.

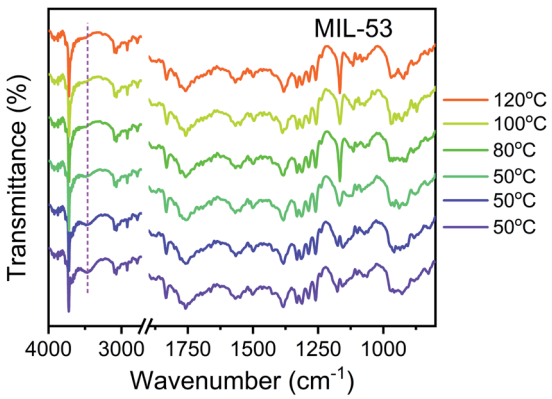

Fig. 11 *In situ* FTIR spectra of MIL-53 at a temperature program from 50 °C to 120 °C.

uptake of ethanediol at 3700–3100 cm^{-1}, pertaining to the stretching mode of OH connected by hydrogen bonding. As anticipated, this peak vanishes after the thermal treatment in vacuum, which reveals that this operation could simultaneously facilitate the desorption of water and ethanediol. By contrast, the characteristic wide vibration peak of O–H···O–H is still remarkable after the thermal treatment of OH–MIL-53 with the uptake of ethanediol (Fig. 12b). It is a sign of additional hydrogen bonding interactions between OH–MIL-53 and ethanediol, which results in the retention of ethanediol in OH–MIL-53.

3.4 Regeneration and cycling utilization of OH–MIL-53

OH–MIL-53 as a polyol adsorbent candidate was further implemented in regeneration and cycling polyol adsorption tests. Polyols on OH–MIL-53 were eluted with ethanol in a Soxhlet extraction setup, and OH–MIL-53 with the uptake of polyols was treated in a hot vacuum oven for regeneration. OH–MIL-53 excels well in the cycling adsorption experiments, in which the uptake of both ethanediol and 1,3-propanediol is almost unchanged after three consecutive adsorption–desorption cycles (Fig. 13).

Our previous report documents that OH–MIL-53 has exceptional hydrothermal stability and tolerance to acidic solution (pH = 4).[38] It is also worth mentioning the good durability of OH–MIL-53. Long-term preservation cannot deactivate its adsorption performance. Following the initial adsorption test, after six months, adsorption cycles 2 and 3 were conducted, and the results still measured up to our expectations (Fig. 13). This feature confirms the utility of the OH–MIL-53 material in industry.

We would like to discuss the energy consumption of adsorption, which determines the prospect of a separation technique to a large extent. Considering the high boiling point of polyols, the desorptive recovery of polyols by elution with volatile solvents, rather than thermally desorptive recovery, might be an option in the future. When replacing water with ethanol, a rough estimation with respect to the heat of evaporation for each gram of solvent demonstrates a reduction in energy consumption of up to 63% for the recovery of pure polyols. This indicates the advantage of adsorption-based separation compared to traditional direct evaporation of a great deal of water from low-concentration polyol systems.

The total energy consumption in the material preparation process, which typically involves the synthesis, activation and regeneration of materials after adsorption, was also estimated, taking OH–MIL-53 as an example. As shown in Fig. 14, we noted that approximately 79% of the electric energy was consumed for the initial reflux synthesis and activation. Comparatively, the consumption of electric energy in the material regeneration accounted for about 21% of the total. This further proves that the recyclability of MOF materials is of great significance for sustainable use in the future.

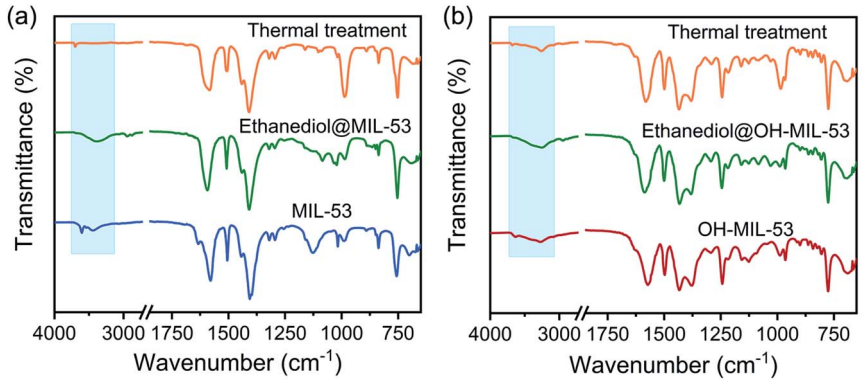

Fig. 12 The FTIR spectra of MIL-53 (a) and OH–MIL-53 (b) after the desorption of ethanediol *via* dynamic vacuum treatment at 120 °C for 5 h.

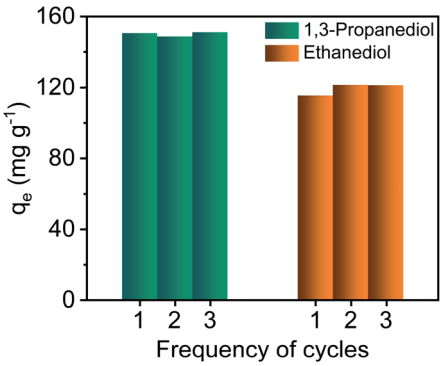

Fig. 13 The cycling of polyol adsorption on OH–MIL-53 at room temperature. The initial concentration of polyol aqueous solution was 200 g L^{-1}.

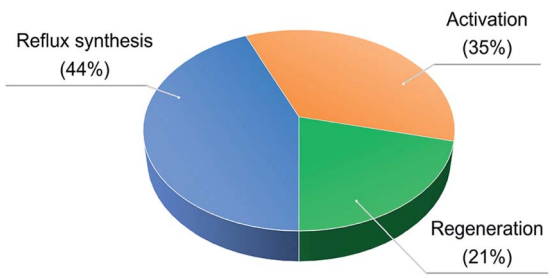

Fig. 14 Electric energy consumption distribution in the OH–MIL-53 preparation process according to the power rating of appliances.

4 Conclusions

MIL-53 and its OH-bonded variants were prepared to explore their potential in polyol adsorption from aqueous solutions. OH–MIL-53 enjoys advantages over MIL-53 and the other OH-bonded variants by virtue of its suitable pore structure and host–guest interactions. Here, we highlight the synergistic effect between two types of host–guest interactions, namely hydrophobic interactions (from alkyl chains) and hydrogen bonding interactions (from OH groups), which drive the impressive polyol adsorption on OH–MIL-53 at a wide concentration range from 10 to 500 g L^{-1}. OH–MIL-53 as a polyol adsorbent is attractive because of its simple synthetic and activation methods, and more importantly, stability and recyclability *via* ethanol elution. These characters uphold the utility of MOFs in real-world liquid separation.

Author contributions

Na Cao: conceptualization, data curation, formal analysis, writing – original draft, writing – review and editing. Jiayi Liu: formal analysis. Yuecheng Wang: formal analysis. Yingwu Zhou: formal analysis. Meng Zhao: formal analysis. Yujie Ban: conceptualization, supervision, writing – review & editing, funding acquisition. Weishen Yang: funding acquisition.

Conflicts of interest

There are no conflicts to declare.

Acknowledgements

This work was supported by the National Natural Science Foundation of China (21978283, 21721004 and 22090063), Youth Innovation Promotion Association of Chinese Academy of Sciences (2021179) and Dalian Institute of Chemical Physics (DICP I201946).

References

1 R. Gérardy, D. P. Debecker, J. Estager, P. Luis and J. C. M. Monbaliu, *Chem. Rev.*, 2020, **120**, 7219–7347.
2 O. Rosales-Calderon and V. Arantes, *Biotechnol. Biofuels*, 2019, **12**, 240.
3 R. K. Saxena, P. Anand, S. Saran and J. Isar, *Biotechnol. Adv.*, 2009, **27**, 895–913.
4 C. L. Cao, H. J. Wang, M. D. Wang, Y. Liu, Z. M. Zhang, S. W. Liang, W. Yuhan, F. S. Pan and Z. Y. Jiang, *J. Membr. Sci.*, 2021, **630**, 119319.

5 Z. M. Zhang, H. Yang, C. L. Cao, Y. Liu, S. W. Liang, M. D. Wang, H. J. Wang, X. Z. Cao, F. S. Pan, H. Wu and Z. Y. Jiang, *J. Membr. Sci.*, 2022, **641**, 119905.
6 M. S. Jyothi, K. R. Reddy, K. Soontarapa, S. Naveen, A. V. Raghu, R. V. Kulkarni, D. P. Suhas, N. P. Shetti, M. N. Nadagouda and T. M. Aminabhavi, *J. Environ. Manage.*, 2019, **242**, 415–429.
7 L. Wang, H. L. Huang, Y. J. Chang and C. L. Zhong, *ACS Sustainable Chem. Eng.*, 2021, **9**, 3195–3202.
8 W. X. Zhang, Y. P. Ying, J. Ma, X. Y. Guo, H. L. Huang, D. H. Liu and C. L. Zhong, *J. Membr. Sci.*, 2017, **527**, 8–17.
9 Y. C. Wang, Y. J. Ban, Z. Y. Hu, Y. Zhao, M. Y. Zheng, W. S. Yang and T. Zhang, *Angew. Chem., Int. Ed.*, 2022, **61**, e202114479.
10 D. L. Crittenden, K. C. Thompson and M. J. T. Jordan, *J. Phys. Chem. A*, 2005, **109**, 2971–2977.
11 H. Jin, Y. S. Li and W. S. Yang, *Ind. Eng. Chem. Res.*, 2018, **57**, 11963–11969.
12 P. M. Stanley, J. Haimerl, C. Thomas, A. Urstoeger, M. Schuster, N. B. Shustova, A. Casini, B. Rieger, J. Warnan and R. A. Fischer, *Angew. Chem., Int. Ed.*, 2021, **60**, 17854–17860.
13 R. Nishiyabu, Y. Kubo, T. D. James and J. S. Fossey, *Chem. Commun.*, 2011, **47**, 1106–1123.
14 X. Wu, X. X. Chen and Y. B. Jiang, *Analyst*, 2017, **142**, 1403–1414.
15 X. T. Zhang, G. J. Liu, Z. W. Ning and G. W. Xing, *Carbohydr. Res.*, 2017, **452**, 129–148.
16 I. Peña, M. E. Sanz, E. R. Alonso and J. L. Alonso, *Chem.–Eur. J.*, 2018, **24**, 13408–13412.
17 G. Oruc, T. Varnali and S. Bekiroglu, *J. Mol. Struct.*, 2018, **1160**, 319–327.
18 E. E. Mallon, A. Bhan and M. Tsapatsis, *J. Phys. Chem. B*, 2010, **114**, 1939–1945.
19 Z. Wang, Z. Wu and T. W. Tan, *Bioresour. Technol.*, 2013, **145**, 37–42.
20 N. Masoumifard, P. M. Arnal, S. Kaliaguine and F. Kleitz, *ChemSusChem*, 2015, **8**, 2093–2105.
21 K. X. Zheng, L. Jiang, S. T. Yu, M. Xian, Z. Q. Song, S. W. Liu and C. Xu, *RSC Adv.*, 2020, **10**, 38085–38096.
22 J. Fortea, L. García, J. Ruiz, M. Oliva and J. Arauzo, *Processes*, 2021, **9**, 1438.
23 S. Kitagawa, R. Kitaura and S. Noro, *Angew. Chem., Int. Ed.*, 2004, **43**, 2334–2375.
24 H. C. Zhou, J. R. Long and O. M. Yaghi, *Chem. Rev.*, 2012, **112**, 673–674.
25 K. C. Jayachandrababu, D. S. Sholl and S. Nair, *J. Am. Chem. Soc.*, 2017, **139**, 5906–5915.
26 R. A. Dodson, A. P. Kalenak and A. J. Matzger, *J. Am. Chem. Soc.*, 2020, **142**, 20806–20813.
27 L. B. Li, R.-B. Lin, R. Krishna, H. Li, S. C. Xiang, H. Wu, J. P. Li, W. Zhou and B. L. Chen, *Science*, 2018, **362**, 443–446.
28 A. E. Baumann, D. A. Burns, B. Q. Liu and V. S. Thoi, *Commun. Chem.*, 2019, **2**, 86.
29 J. P. Zhang, H. L. Zhou, D. D. Zhou, P. Q. Liao and X. M. Chen, *Natl. Sci. Rev.*, 2018, **5**, 907–919.
30 A. Cadiau, Y. Belmabkhout, K. Adil, P. M. Bhatt, R. S. Pillai, A. Shkurenko, C. Martineau-Corcos, G. Maurin and M. Eddaoudi, *Science*, 2017, **356**, 731–735.
31 F. Jiménez-Cruz, J. A. Hernández, G. C. Laredo, M. T. Mares-Gallardo and J. L. García-Gutierrez, *Energy Fuels*, 2007, **21**, 2929–2934.
32 H. N. Tran, Y. F. Wang, S. J. You and H. P. Chao, *Process Saf. Environ. Prot.*, 2017, **107**, 168–180.
33 M. Sarker, H. J. An and S. H. Jhung, *J. Phys. Chem. C*, 2018, **122**, 4532–4539.
34 M. Amirilargani, R. B. Merlet, P. Hedayati, A. Nijmeijer, L. Winnubst, L. C. P. M. de Smet and E. J. R. Sudhölter, *Chem. Commun.*, 2019, **55**, 4119–4122.
35 D. Himsl, D. Wallacher and M. Hartmann, *Angew. Chem., Int. Ed.*, 2009, **48**, 4639–4642.
36 T. Kundu, B. B. Shah, L. Bolinois and D. Zhao, *Chem. Mater.*, 2019, **31**, 2842–2847.
37 C. L. Kong, H. B. Du, L. Chen and B. L. Chen, *Energy Environ. Sci.*, 2017, **10**, 1812–1819.
38 N. Cao, H. L. Wang, Y. J. Ban, Y. C. Wang, K. Yang, Y. W. Zhou, M. Zhao, W. Q. Deng and W. S. Yang, *Angew. Chem., Int. Ed.*, 2021, **60**, 1629–1634.
39 S. Z. Wang, H. F. Dai, Z. P. Yan, C. J. Zhu, L. F. Huang and B. S. Fang, *Eng. Life Sci.*, 2014, **14**, 485–492.
40 Y. X. Jia, W. Z. Sun, C. Yin, C. Xu, S. T. Yu and X. Mo, *J. Chem. Technol. Biotechnol.*, 2019, **94**, 1259–1268.